7 Appendix: Derivation of some important model equations

The derivation of the *basic* formulation of the generalized ICCR (GICCR) [16] requires the following assumptions:

- A one-dimensional transistor structure is considered, with the emitter contact at the monosilicon surface and the collector contact at the transition from the “lightly”-doped collector region to the buried layer. The vertical ordinate is designated with x and is omitted in the following derivation from the indices for reasons of better legibility and understanding.
- The volume recombination in above region is negligible.
- The time derivative is zero; in general, it is sufficient though to assume quasi-static operation.
- Effects such as thermionic emission and tunneling across the junctions are neglected; they need to be accounted for by separate terms and can - in principle - be combined with the GICCR solution.

It can be shown that a GICCR can also be derived for the a three-dimensional case, so that the assumption of a one-dimensional region can be dropped for a actual applications.

First, consider the electron continuity equation which, together with the second and third assumption, reads

$$\frac{dJ_n}{dx} = q\left(R + \frac{\partial n}{\partial t}\right) = 0 \ . \tag{7.0.0-1}$$

This corresponds to a spatially independent electron current density,

$$J_n = const(x) = -J_T = \frac{-I_T}{A_E} \ , \tag{7.0.0-2}$$

which can be expressed by the transfer current and area of the (1D) transistor. Note, that under DC operation, $I_T = I_C$.

The derivation starts with the electron transport equation:

$$J_n = -q\mu_n n\frac{d\varphi_n}{dx} \tag{7.0.0-3}$$

Inserting the electron density,

$$n = n_i \exp\left(\frac{\psi - \varphi_n}{V_T}\right) \tag{7.0.0-4}$$

gives

$$J_n = -q\mu_n n_i \exp\left(\frac{\psi - \varphi_n}{V_T}\right)\frac{d\varphi_n}{dx} = -q\mu_n n_i \exp\left(\frac{\psi}{V_T}\right)\exp\left(-\frac{\varphi_n}{V_T}\right)\frac{d\varphi_n}{dx} \ . \tag{7.0.0-5}$$

Note, that n_i is the effective intrinsic carrier density; it contains for the various transistor regions possible bandgap differences, that are caused by high-doping effects and bandgap-engineering. This topic will be discussed later.

Using

$$\frac{d\left(\exp\left(-\frac{\varphi_n}{V_T}\right)\right)}{dx} = -\frac{1}{V_T}\exp\left(-\frac{\varphi_n}{V_T}\right)\frac{d\varphi_n}{dx} \tag{7.0.0-6}$$

leads to

$$J_n = qV_T\mu_n n_i \exp\left(\frac{\psi}{V_T}\right)\frac{d\left(\exp\left(-\frac{\varphi_n}{V_T}\right)\right)}{dx} \ . \tag{7.0.0-7}$$

Separation of the differential terms gives

$$\frac{J_n}{qV_T\mu_n n_i}\exp\left(-\frac{\psi}{V_T}\right)dx = d\left(\exp\left(-\frac{\varphi_n}{V_T}\right)\right) \ . \tag{7.0.0-8}$$

The inconvenient term $\exp(-\psi/V_T)$ can be replaced by more useful variables such as the hole density and an $\exp(\varphi_p/V_T)$ term via the transformation,

$$\exp\left(-\frac{\psi}{V_T}\right) = \frac{n_i \exp\left(\frac{\varphi_p - \psi}{V_T}\right)}{n_i \exp\left(\frac{\varphi_p}{V_T}\right)} = \frac{p}{n_i \exp\left(\frac{\varphi_p}{V_T}\right)} \ , \tag{7.0.0-9}$$

yielding

$$\frac{J_n}{qV_T}\frac{p}{\mu_n n_i^2 \exp\left(\frac{\varphi_p}{V_T}\right)}dx = d\left(\exp\left(-\frac{\varphi_n}{V_T}\right)\right) \tag{7.0.0-10}$$

Integration of the above equation over the interval $[x_l, x_u]$ gives:

$$\int_{x_l}^{x_u}\frac{J_n}{qV_T}\frac{p}{\mu_n n_i^2 \exp\left(\frac{\varphi_p}{V_T}\right)}dx = \int_{\exp(\varphi_n(x_l)/V_T)}^{\exp(\varphi_n(x_u)/V_T)} d\left(\exp\left(-\frac{\varphi_n}{V_T}\right)\right) \tag{7.0.0-11}$$

The result for the right-hand-side is

$$\int_{\exp(\varphi_n(x_l)/V_T)}^{\exp(\varphi_n(x_u)/V_T)} d\left(\exp\left(-\frac{\varphi_n}{V_T}\right)\right) = -\left[\exp\left(-\frac{\varphi_n(x_u)}{V_T}\right) - \exp\left(-\frac{\varphi_n(x_l)}{V_T}\right)\right] . \tag{7.0.0-12}$$

The exact value of the electron quasi-fermi potentials depends on the choice of the integration limits and will be discussed later. First, the left-hand-side of (7.0.0-12) is integrated, giving after extension with the exp of the controlling (internal) base-emitter voltage, exp(-V_{BEi}/V_T), and with the transfer current density as defined in (7.0.0-2) the general expression

$$\int_{x_l}^{x_u}\frac{J_n}{qV_T}\frac{p}{\mu_n n_i^2 \exp\left(\frac{\varphi_p}{V_T}\right)}dx = \frac{J_T \exp\left(-\frac{V_{BEi}}{V_T}\right)}{qV_T}\int_{x_l}^{x_u}\frac{p}{\mu_n n_i^2}\frac{J_n}{J_T}\exp\left(\frac{V_{BEi}-\varphi_p}{V_T}\right)dx , \tag{7.0.0-13}$$

that contains the desired terminal variables of the 1D transistor. The reason for not using (7.0.0-2) and $\varphi_p = V_{BEi}$ directly is the yet undefined integration interval. Equating again (7.0.0-13) and (7.0.0-12), and keeping only the desired variable J_T on the l.h.s., results in the general basic formulation

$$J_T = qV_T \frac{\exp\left(\frac{V_{BEi}}{V_T}\right)\left[\exp\left(-\frac{\varphi_n(x_l)}{V_T}\right) - \exp\left(-\frac{\varphi_n(x_u)}{V_T}\right)\right]}{\int_{x_l}^{x_u} \frac{p}{\mu_n n_i^2}\frac{J_n}{J_T}\exp\left(\frac{V_{BEi}-\varphi_p}{V_T}\right)dx} \quad , \tag{7.0.0-14}$$

from which different forms of the ICCR can be derived. At this point, the various terms and variables as well as the choice of the integration limits need to be discussed in order to enable the derivation of a practically more applicable relation than the above one.

The electron fermi-potentials in the numerator assume their known 1D terminal values only at the contacts, i.e. if the entire 1D transistor region $[x_E, x_C]$ is chosen as integration interval,

$$\varphi_n(x_l) = \varphi_n(x_E) = 0 \quad \text{and} \quad \varphi_n(x_u) = \varphi_n(x_C) = V_{CEi} \ , \tag{7.0.0-15}$$

making this an attractive choice, the effect of which on the denominator is discussed next.

Defining the spatially dependent weighting function in normalized form,

$$h(x) = \underbrace{\frac{\mu_{n0r} n_{ir}^2}{\mu_n(x) n_i^2(x)}}_{h_g} \underbrace{\frac{J_n(x)}{J_T}}_{h_i} \underbrace{\exp\left(\frac{V_{BEi}-\varphi_p(x)}{V_T}\right)}_{h_v} = h_g\, h_i\, h_v g \tag{7.0.0-16}$$

with μ_{n0r} and n_{ir} as mobility and intrinsic carrier density, respectively, of a reference material (e.g. the base or a point in the base region), permits to write the denominator as

$$\int_{x_E}^{x_C} \frac{p}{\mu_n n_i^2}\frac{J_n}{J_T}\exp\left(\frac{V_{BEi}-\varphi_p}{V_T}\right)dx = \frac{1}{\mu_{n0r} n_{ir}^2}\int_{x_E}^{x_C} h(x)p(x)dx \ . \tag{7.0.0-17}$$

For any bias point, the integral on the r.h.s., multiplied by q, can *always* be written as

$$q\int_{x_E}^{x_C} h(x)p(x)dx = \bar{h}\overline{Q}_p \ , \tag{7.0.0-18}$$

with $\bar{h}$ as an average value of the weighting function and

$$\overline{Q}_p = q\int_{x_l}^{x_u} p(x)dx \tag{7.0.0-19}$$

is the 1D (i.e. per area) hole charge stored in the selected integration interval. The latter can be measured via the terminals if the integration interval is chosen properly.

A brief discussion of the weighting function follows in order to provide a better idea of the assumptions made for the ICCR and GICCR.

The weighting function h_v

The hole quasi-fermi potential is equal to V_{BEi} at least over the base and its adjacent space charge regions as well as far into the emitter and collector region, resulting in $h_v = 1$ within the respective integration interval. This is also true in the very thin emitter region of advanced transistors. In conventional processes with larger emitter junction depth though, a significant portion of the holes injected back into the neutral emitter recombine there, leading to a slight decrease of φ_p. However, the resulting deviation of h_v from 1 within this region coincides with a rapid decrease of holes, so that the contribution of the product $h*p$ to the integral is negligible. Therefore, $h_v = 1$ is a very good assumption under all relevant bias conditions.

The weighting function h_i

The transfer current density (at the 1D collector contact) equals the electron current density in the base and collector region. Only in the BE space-charge region and the neutral emitter region, J_n can increase slightly as a result of the back injection of holes and the corresponding recombination. The maximum increase occurs at the emitter contact x_E:

$$J_n(x_E) = J_T + J_p(x_E)\,. \tag{7.0.0-20}$$

The maximum possible increase occurs for opaque emitters, where $J_p(x_E) = J_B$, and is given by

$$max\{h_i\} = h_i(x_E) = 1 + \frac{J_B}{J_T} = 1 + \frac{1}{B} \tag{7.0.0-21}$$

with B as the DC current gain. As a consequence, for the vast majority and, particularly advanced bipolar transistors, $h_i = 1$ is a good assumption under all relevant bias conditions.

The weighting function h_g

High-doping effects as well as intentional bandgap grading in heterojunction transistors can cause n_i^2 values to differ by orders of magnitude in the various transistor regions. In addition, also the mobility varies significantly within the transistor as a function of both doping and bias (via the electric field). The variation caused by the latter is most pronounced in the BC junction and collector region. In general though, μ_n and n_i possess an opposite dependence on doping, leading to a partial compensation within h_g. However, the influence of n_i still remains much stronger than that of μ_n. As a consequence, the weighting function h_g deviates strongly from 1 and has to be considered for all processes. Note, that the index "g" has been chosen to indicate the major factor of influence, namely the bandgap in the effective intrinsic carrier concentration. Nevertheless, a spatially dependent function h_g can still be accommodated in a compact model formulation as shown below.

Overall, for properly designed transistors the weighting function h consists only of the contribution of h_g, so that the average value in (7.0.0-18) is given by

$$\bar{h} = \bar{h}_g = \frac{\mu_{n0r} n_{ir}^2}{\overline{\mu_n n_i^2}} \; . \qquad (7.0.0\text{-}22)$$

Note that the bias dependence of $\bar{h}$ can also be caused by a bias dependent hole distribution within the transistor, even if $h(x)$ does not depend on bias; e.g., at high current densities, $p(x)$ can spread into the collector in which n_i^2 might be few orders of magnitude smaller than in the base, so that the collector portion of the hole charge has to be weighted much stronger than the base portion and can, therefore, still cause a significant contribution to the overall integral, although the charge in the collector might still be very small [16]!

Since the major contribution to the integral comes from the base region, where the hole density is largest, the only other relevant contributions will come from those regions, where the hole den-

sity has not dropped to insignificant values. In other words, the regions towards the contacts do not contribute to the integral and are irrelevant for the discussion on how to chose the integration interval for the denominator of (7.0.0-14). Of the infinite number of possible integration intervals, the two most important choices are:

- If the base region is chosen as integration interval, $\bar{h}$ can be shown to be only very weakly bias dependent for homojunction transistors. The main disadvantages, however, are (i) the unknown and strongly bias dependent values for the electron quasi-fermi potentials at the base region boundaries, which are not easily accessible by measurements, and (ii) the difficulty to measure the base hole charge separately (and to extract the corresponding model parameters). In addition, the bias dependence of $\bar{h}$ will not be as weakly dependent anymore for drift HBTs.
- If the entire 1D transistor region is chosen as integration interval, $\bar{h}$ is expected to exhibit a larger bias dependence than for homojunction transistors. It has been shown though for bipolar technologies over (at least) the past 25 years that the bias dependence of $\bar{h}$ is negligible in the bias region of practical interest. As an advantage of choosing the 1D contacts for boundary conditions, the electron quasi-fermi potentials are well-known and given by (7.0.0-15).

For the reasons given above, the entire (1D) transistor region has been chosen as integration interval. The resulting transfer current expression then reads

$$J_T = qV_T \frac{\exp\left(\frac{V_{BEi}}{V_T}\right) - \exp\left(\frac{V_{BCi}}{V_T}\right)}{\int_{x_E}^{x_C} \frac{p}{\mu_n n_i^2} dx} , \tag{7.0.0-23}$$

or after introducing the weighting function h_g according to (7.0.0-16)

$$J_T = q^2 V_T \mu_{n0r} n_{ir}^2 \frac{\exp\left(\frac{V_{BEi}}{V_T}\right) - \exp\left(\frac{V_{BCi}}{V_T}\right)}{q\int_{x_E}^{x_C} \frac{\mu_{n0r} n_{ir}^2}{\mu_n n_i^2} p\, dx} . \tag{7.0.0-24}$$

7.1 The ICCR (homojunction transistors)

Inserting (7.0.0-15), (7.0.0-18) with $\bar{h} = \bar{h}_g$ as well as $V_{BCi} = V_{BEi}$-V_{CEi} into (7.0.0-14) yields

$$J_T = q^2 V_T \overline{\mu_n n_i^2} \frac{\exp\left(\frac{V_{BEi}}{V_T}\right) - \exp\left(\frac{V_{BCi}}{V_T}\right)}{\bar{Q}_p} \quad . \tag{7.1.0-25}$$

This equation, with

$$c_{10} = q^2 V_T \overline{\mu_n n_i^2} \tag{7.1.0-26}$$

is the well-known ICCR, which is very accurate for most homojunction transistors, provided that the hole charge (density),

$$\bar{Q}_p = \bar{Q}_{p0} + \bar{Q}_{jEi} + \bar{Q}_{jCi} + \bar{Q}_f + \bar{Q}_r \tag{7.1.0-27}$$

is accurately modeled as a function of bias. The latter is a prerequisite for the description of high-speed applications in any way. Also, since the hole charge has to be continuously differentiable with respect to bias, the transfer current is also automatically continuously differentiable over all bias regions and is modeled via a single-piece formulation.

Fig. illustrates the impact of the various hole charges on the transfer current during a sweep of the BE voltage. At low current densities, the depletion charges Q_{jEi} and Q_{jCi} are the only bias dependet contributors to Q_p. For constant V_{BC}, the bias dependence of the BE depletion charge determines the ideality of the transfer current charectristic; for constant V_{BC}, the bias dependence of the BC depletion charge determines the slope of the output characteristics and, thus, automatically takes into account the bias dependent Early voltage. At high current densities, the minority charge Q_f starts to increase rapidly exceeding the depletion charges around peak f_T and then dominating the bias dependence of Q_p beyond peak f_T. As a consequence, the ideality factor of the transfer current characteristic also increases rapidly leading to a string decrease in the transcondutance. A detailed discussion of the ICCR for BJT processes can be found in, e.g., [5].

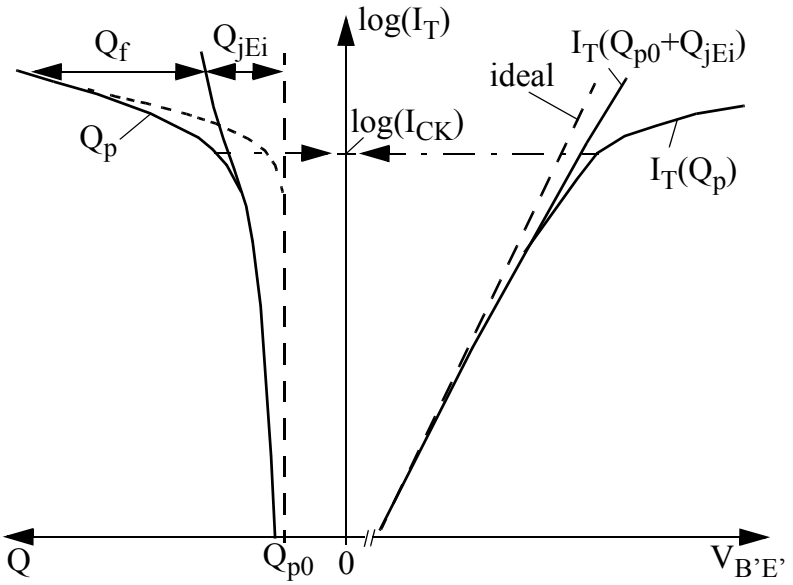

Fig. 7.1.0/1: Illustration of the impact of the various charge components on the transfer current, calculated by the ICCR.

7.2 The GICCR (heterojunction transistors)

In homojunction transistors bandgap differences are caused by high-doping effects only, so that the variation in n_i^2 over the integration interval $[x_E, x_C]$ is moderate. In contrast, large bandgap differences are intentional in HBTs, leading to n_i^2 variations of orders of magnitude. As demonstrated in [36], the transfer current of (SiGe) HBTs cannot be described anymore with the ICCR. The latter can be extended though, resulting in the generalized ICCR (GICCR) which maintains the advantages of a single-piece continuously differentiable description of the main transistor current. While the integration interval and, thus, the numerator of (7.0.0-14) remain the same, the denominator of (7.0.0-14) has to be considered more carefully for HBTs.

The starting point for the extension is eq. (7.0.0-17), with $h(x) \approx h_g(x)$ for the same reasons as discussed before, resulting in

$$\int_{x_E}^{x_C} \frac{p}{\mu_n n_i^2} dx = \frac{1}{\mu_{n0r} n_{ir}^2} \int_{x_E}^{x_C} \frac{\mu_{n0r} n_{ir}^2}{\mu_n n_i^2} p(x) dx \ . \qquad (7.2.0\text{-}28)$$

The choice of the reference material (or reference transistor region) and its associated parameter values for $\mu_{n0r} n_{ir}^2$ is arbitrary and will be discussed later. Due to the large variation of n_i^2 between emitter, base and collector region, the definition of a sufficiently bias independent average value $\overline{h_g}$ is not always possible and might lead to unacceptable errors in modeling the transfer current high current densities. The goal is, therefore, to formulate the integral in terms of single charges in particular transistor regions, multiplied with proper average values of the respective weighting functions, that are both suitable for compact modeling.

In HBTs, the bandgap is significantly different in the emitter, base and collector region, while the transition from one bandgap to another usually takes place around the junction. As a consequence, partitioning of the integral into the neutral emitter, base and collector region as well as into depletion regions looks like a reasonable choice in order to obtain separate integrals in which the weighting functions are sufficiently independent on location and bias. Defining the respective average values,

$$\bar{h}_k = \bar{h}_{gk} = \frac{\int h_{gk} p(x) dx}{\int p(x) dx} = \frac{\mu_{n0r} n_{ir}^2}{\overline{\mu_{nk} n_{ik}^2}} \quad \text{with k = (e, jei, b, jci, c)}, \tag{7.2.0-29}$$

the denominator integral of the ICCR reads after multiplying with q

$$\overline{Q}_{p,T} = q \int_{x_E}^{x_C} \frac{\mu_{n0r} n_{ir}^2}{\mu_n n_i^2} p(x) dx = \overline{Q}_{p0} + h_{jEi} \overline{Q}_{jEi} + h_{jCi} \overline{Q}_{jCi} + \overline{Q}_{f,T} + \overline{Q}_{r,T} \,. \tag{7.2.0-30}$$

where the base region has been chosen as reference, i.e. $\mu_{n0r} n_{ir}^2 = \overline{\mu_{nb} n_{ib}^2}$. According to [36], assuming bias independent average values for the separate weighting functions leads to a significant improvement over the conventional ICCR with a sufficiently accurate description of the transfer current characteristics and the respective derivatives over the entire bias range of interest (up to very high current densities). The average weighting factors are new model parameters.

Application of the GICCR also requires the modeling of the separate portions, $\overline{Q}_{pE}$ and $\overline{Q}_{pC}$, of the total hole charge. The GICCR has been evaluated for many advanced SiGe bipolar technolo-

gies. It has been found that a constant factor $\bar{h}$ can in fact be used for more than one bias point up to quite high current densities, thus maintaining all the advantages of the ICCR with the added benefit of being able to model HBTs in physics-based way.

For a 2D/3D GICCR, see [74].

7.3 Vertical NQS effects implementation

Non-quasi-static behavior results from temporally and spatially distributed effects within the transistor structure. Therefore, theoretical treatment requires the solution of the continuity *and* transport equation. Under certain simplifications regarding the transistor structure and assuming small-signal operation, the corresponding second-order differential equation can be solved in one dimension and in frequency domain. Truncating the solution after the second frequency term reads,

$$\underline{X}_{nqs} \approx X_{qs} - (\omega\tau_2)^2 - j\omega\tau_1 \text{ with } (\underline{X} = \underline{I}_\mathrm{T}, \underline{Q}_\mathrm{f}), \tag{7.3.0-31}$$

which is valid at each bias point. $\underline{X}_\mathrm{qs}$ is the corresponding quasi-static value; τ_1 and τ_2 are time constants, and ω is the radian frequency. Converting the frequency-domain solution $\underline{X}$ to a slightly different form (with $s = j\omega$),

$$\frac{\underline{X}_{T,\,NQS}(\omega)}{\underline{X}_T} = 1 - s\tau_1 + (s\tau_2)^2 \cong \frac{1}{1 + A_1 s + A_2 s^2}, \tag{7.3.0-32}$$

which is valid for not too high frequencies, allows to apply Laplace transformation in order to obtain the corresponding time-domain approximation,

$$A_2 \frac{d^2 x_{T,\,NQS}}{dt^2} + A_1 \frac{dx_{T,\,NQS}}{dt} + x_{T,\,NQS} = x_T(t), \; x = (i_T, Q_f). \tag{7.3.0-33}$$

This transformation is always valid as long as the linearized small-signal case is also considered in time-domain. The form of the obtained 2nd-order differential equation resembles the existing time-domain solution. If (7.3.0-33) is interpreted as Bessel polynomial by simply choosing A_2 slightly differently from its expression that would result from the physics-based solution (7.3.0-32),

it was shown in [76] that the above system accomplishes in both domains the task of properly shifting the terminal currents as a consequence of NQS effects. The change of A_2 is correlated with A_1 and, thus, τ_1. As a consequence, only the first-order time constants ("delay times") are required for modeling. This is demonstrated in Fig. 7.3.0/2, in which (7.3.0-32) is compared to the small-signal results from 1D device simulation. The conversion $1\text{-}X \rightarrow (1+X)^{-1}$ in (7.3.0-32) along with the 2nd-order term enables the magnitude to follow the physically correct drop rather than to increase. The form $(1+X)^{-1}$ is in fact more accurate over a wider frequency range or, in other words, allows to compensate for ignoring higher order terms of the original physics-based solution. Note, that the impact of C_{jCi} on the results is negligible at the selected high current density bias point. This example shows that the above transformation system not only is consistent in frequency- and time-domain but also yields accurate results. For comparison, also the partitioned charge-based (PCB) model is shown with its incorrect description of both base current (i.e. input admittance) and magnitude of the collector current (i.e. transconductance).

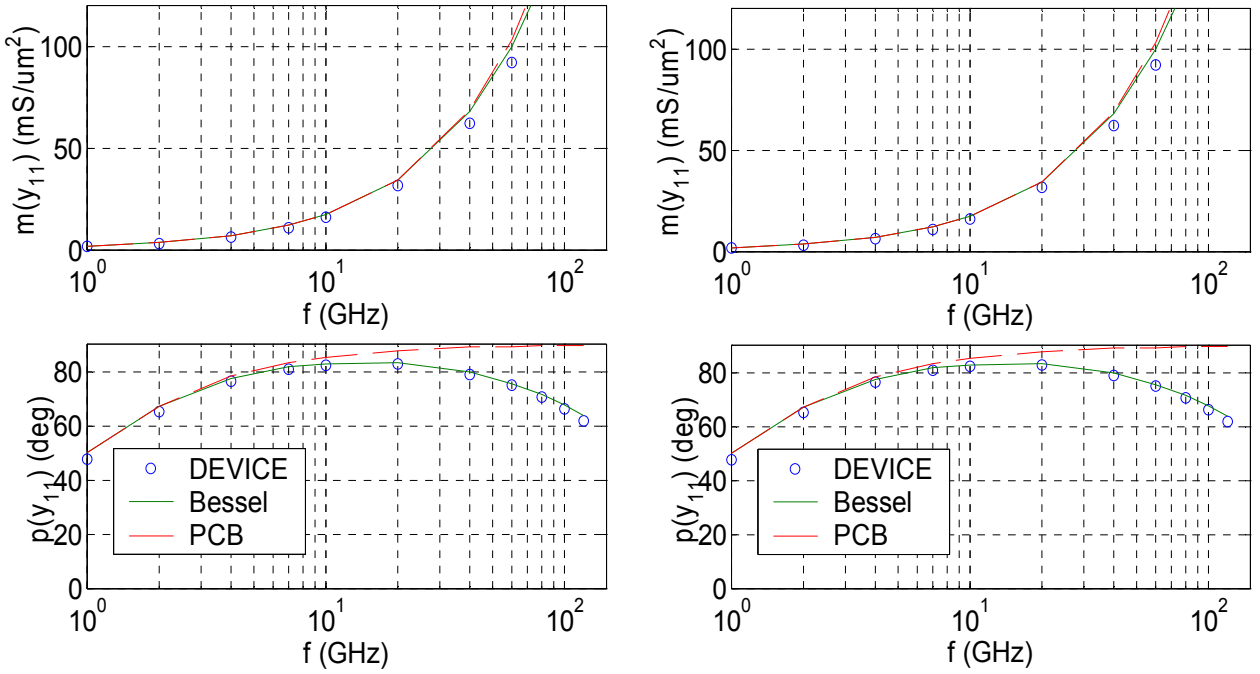

Fig. 7.3.0/2:(a) Input admittance and (b) transadmittance of a 100GHz SiGe HBT: Comparison of (7.3.0-32) with AC device simulation results. Bias point: $J_C = 6.1\text{mA}/\mu\text{m}^2$ ($V_{B'E'} = 0.922\text{V}$) and $V_{B'C'} = 0\text{V}$.

As shown in Fig. 7.3.0/3, the delay times, as calculated from device simulation, increase with bias current and are proportional to the transit time. Therefore, for each bias point, the proper delay time has to be inserted.

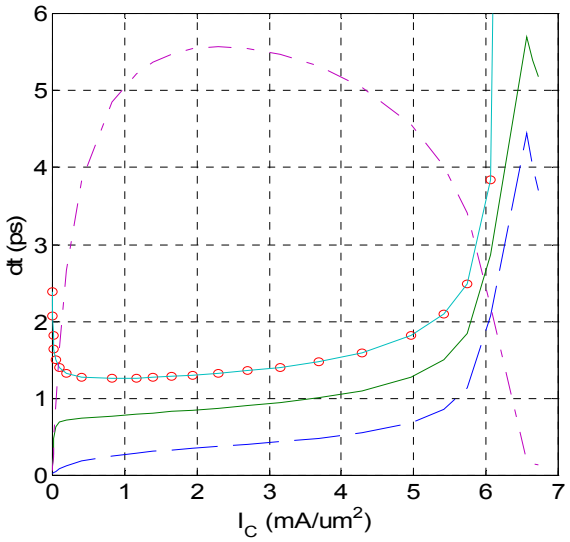

Fig. 7.3.0/3: NQS delay times τ_{IT} (solid green line) and τ_{Qf} (dashed blue line) vs. bias current for the CED HBT. For reference, the accumulated transit time $\tau_{m\Sigma}$ (line with circles) from Regional Analysis as well as f_T (dash-dotted red line) have been inserted.

For general large-signal operation no analytical solution exists. Observation from device simulation and measurements at medium and high-current densities for both sinusoidal and pulse signals with several 100mV amplitude indicates that there is no fundamental difference in the NQS behavior. In other words, the terminal currents react delayed w.r.t. the input voltage. Thus, the 2nd-order differential equation should still be applicable to accomplish the delay. In practice, transient simulation consists of a sequence of circuit equation system solutions at discrete time points. The change between time points is generally small enough to consider the theoretical solution as a sufficiently accurate representation, if just the time constants at each time (i.e. bias) point are inserted. In other words, the linearized delay transformation form (7.3.0-33) is applied to each time point. The accuracy of this approach has been demonstrated numerous times by examples ranging from device simulation to production circuit design.

The expression (7.3.0-33) can be implemented in a circuit simulator with an LCR network or its corresponding gyrator equivalent [77], as shown in Fig. 7.3.0/4. The gyrator network avoids inductors which is advantageous in certain circuit simulators.

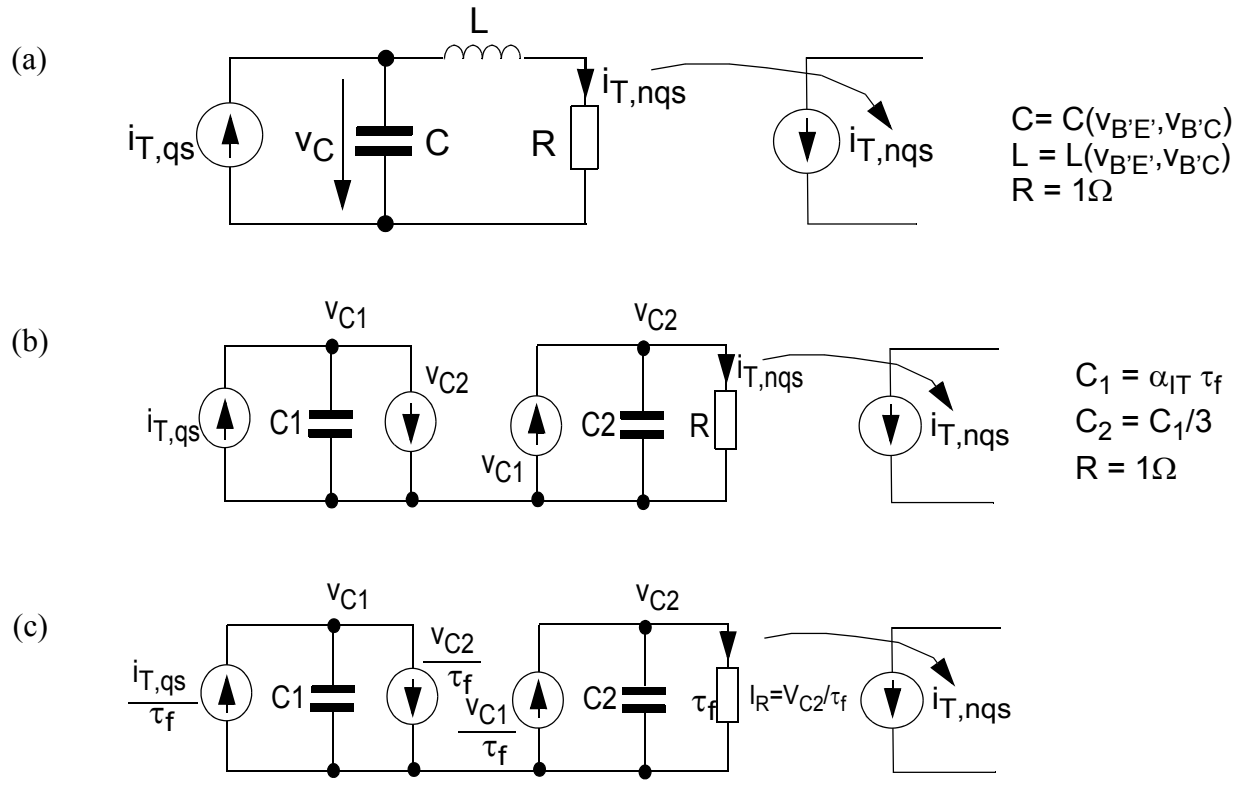

Fig. 7.3.0/4: (a) Adjunct LCR network for describing NQS effects of the transfer current i_T (a similar circuit holds for the minority charge Q_f). (b) Gyrator equivalent of LCR circuit in (a). (c) Gyrator equivalent circuit with normalization to the (normalized) transit time in order to eliminate the undesired derivatives due to the bias dependence.

Since the response of the LCR adjunct network represents the desired physics-based solutions exactly ***in time and frequency domain***, the network has been employed for implementing ***NQS effects*** in HICUM via ***Verilog-A***, which does not permit the implementation via Weil's approach anymore. Unfortunately, a straight-forward implementation is not possible since the bias dependence of the delay times causes the model compiler to create undesired derivatives in the small-signal network. Although these derivatives are mathematically correct, they simply result from a physically inadequate representation of the NQS effect through the adjunct network.

In order to overcome the derivative issue, the equations of the networks had to be modified according to Fig. 7.3.0/4(c). In Fig. 7.3.0/4(c), using KCL at node 1 and 2, one can write in case of a bias dependent transit time τ_f the following equations,

$$\left(\frac{I_{T,qs} - V_{C2}}{\tau_f}\right) = \frac{d}{dt}(\alpha_{IT} V_{C1}), \tag{7.3.0-34}$$

$$\left(\frac{V_{C1} - V_{C2}}{\tau_f}\right) = \frac{d}{dt}\left(\frac{\alpha_{IT}}{3} V_{C1}\right). \tag{7.3.0-35}$$

The above equations effectively make the capacitive elements bias-independent and, hence, remove the generation of undesired derivatives [78]. The same trick has been used for the corresponding minority charge related network.

The overall equivalent circuit for HICUM/L2 has been extended with two adjunct networks for the NQS effects in i_T and for Q_f, respectively. The corresponding Verilog-A implementation has been verified against the built-in HICUM/L2 version 2.1 in SPECTRE, which uses Weil's approach for the implementation. The following Fig. 7.3.0/5 shows the collector and base current waveforms for a 20ps pulse applied at the base of the transistor. As reference and to estimate deviations from possibly different time steppings during the transient, the quasi-static results have also been inserted. The plots are showing good agreement for NQS results.

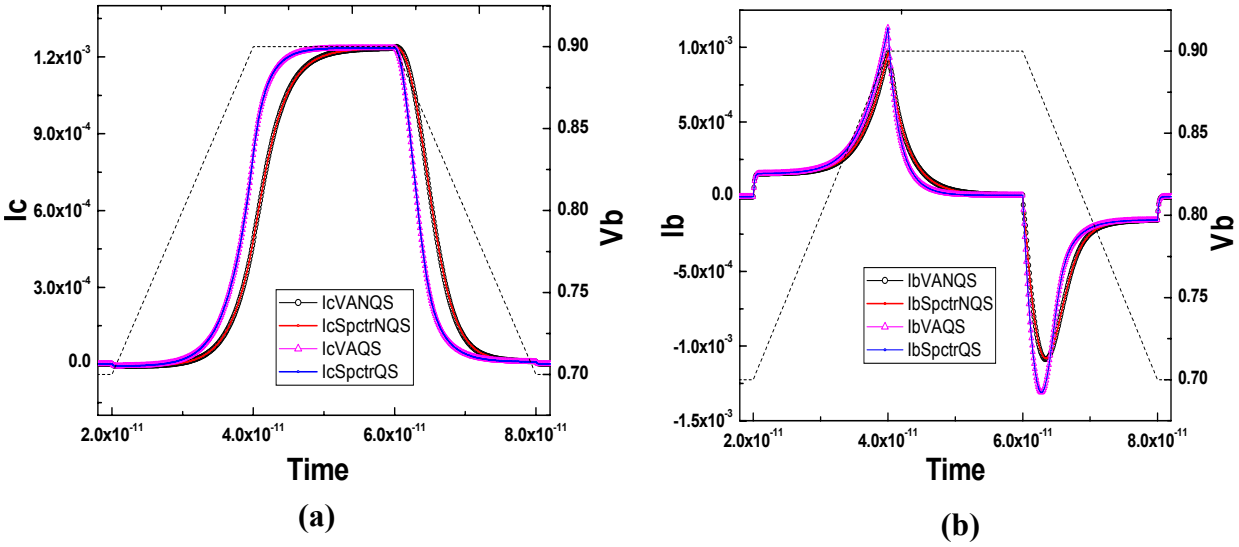

Fig. 7.3.0/5: Time dependence of the collector current (a) and base current (b) in response to a voltage input pulse (dotted line): comparison between v2.23 VA code with NQS networks (solid line with diamonds), v2.1 in SPECTRE with Weil's implementation (solid red line). For reference, the quasi-static results are also inserted for VA v2.23 (large diamonds) and v2.1 in SPECTRE (blue solid line). Units are [A] for currents, [V] for voltages, [s] for time.

Further testing has been performed using a smooth input pulse (rather than a ramp with its discontinuities) in order to rule out any time stepping related discrepancies. The time dependence of the pulse was calculated as

$$s(t) = S_{max}[1 - e^{-(t/\tau)^2}], \tag{7.3.0-36}$$

with the time constant

$$\tau = \frac{\sqrt{2/e}}{2\pi f} \quad , \tag{7.3.0-37}$$

where S_{max} is the maximum amplitude of the pulse and f is the frequency in Hz. The results in Fig. 7.3.0/6 show a very good agreement than for the ramp also. Note that for smooth signals the same accuracy as for discontinuous signals is obtained with a much smaller number of time points.

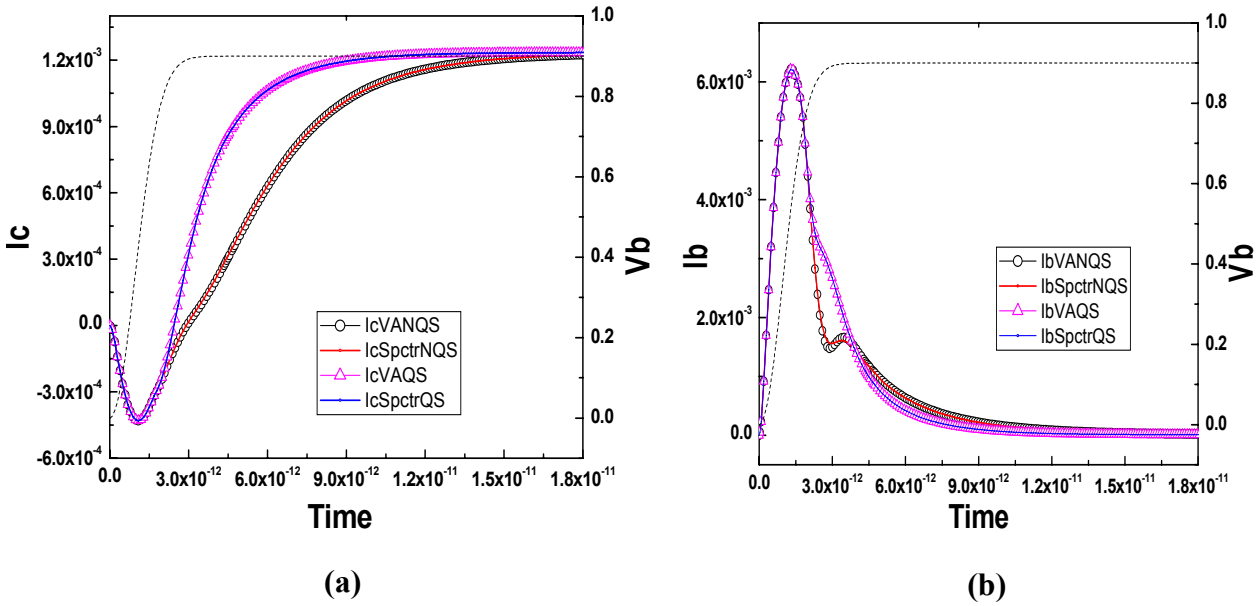

(a) **(b)**

Fig. 7.3.0/6: Time dependence of the collector current (a) and base current (b) in response to a smooth voltage input pulse (dotted line) with a maximum slope corresponding to a frequency of 100GHz: Comparison between v2.23 VA code with NQS networks (solid black line with circles), v2.1 in SPECTRE with Weil's implementation (solid red line). For reference, the quasi-static results are also inserted for VA v2.23 (triangles) and v2.1 in SPECTRE (blue solid line).

Frequency domain results in terms of small-signal y-parameters are shown in Fig. 7.3.0/7. As expected and desired, mostly the phase is altered by the NQS effects, and the magnitudes show the physically correct behaviour. NQS effects have no impact on the inverse y parameters.

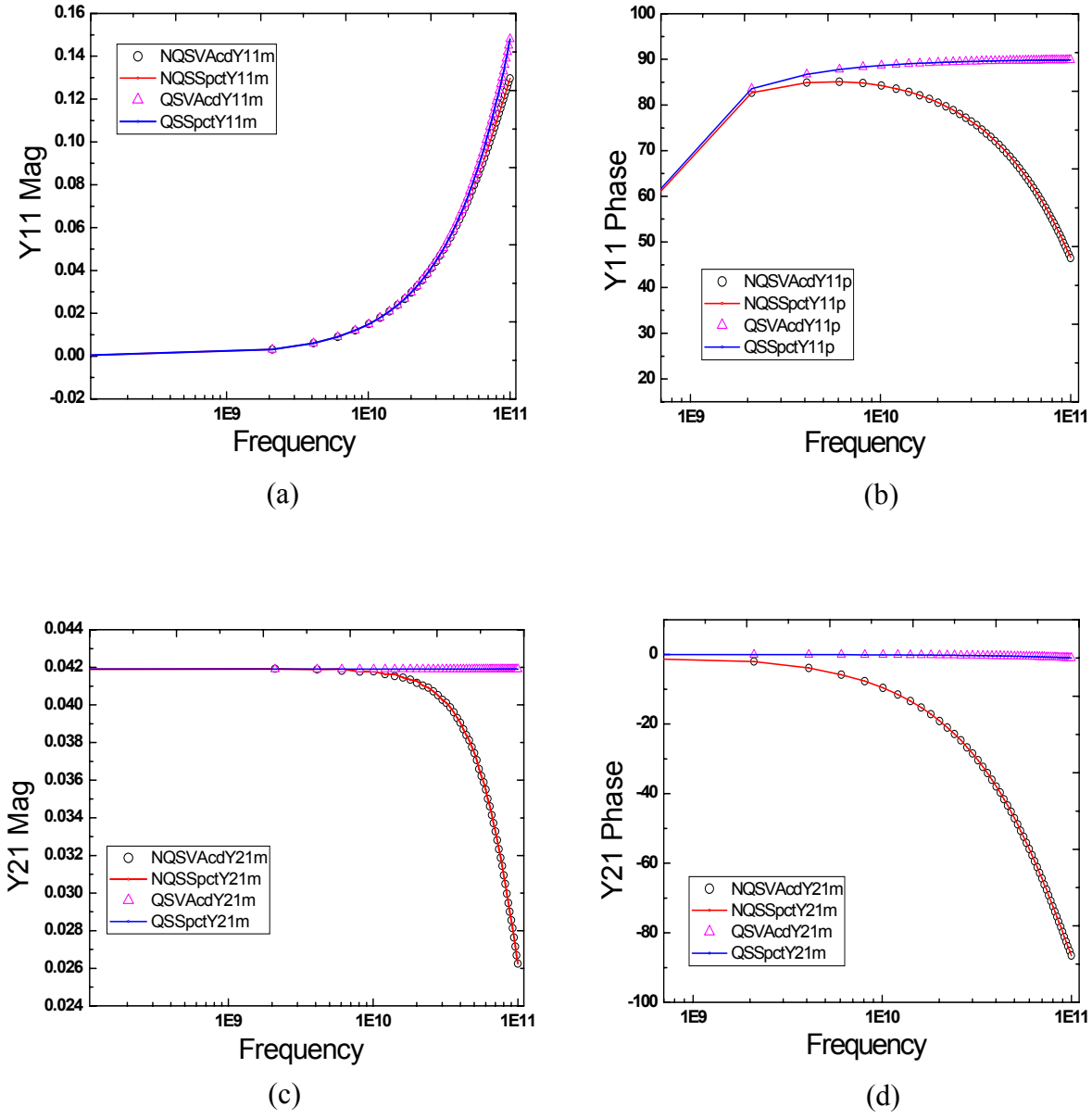

Fig. 7.3.0/7: Small-signal forward y-parameters for V_{BE} = 0.9V and V_{CE} = 0.9V: comparison between v2.23 VA code with NQS networks (diamonds), v2.1 in SPECTRE with Weil's implementation (solid red line). For reference, the quasi-static results are also inserted for VA v2.23 (triangles) and v2.1 in SPECTRE (blue solid line).

7.4 Lateral NQS effects.

Starting with v2.22, in the expression for C_{rBi} the contributions related to C_{dei} and C_{dci} have been included w.r.t. the proper node voltages. This has been possible due to the implementation of ***ddx*** operator in most of the model compilers:

$$C_{rBi} = f_{crBi} ddx(Q_{jEi}, V(bi)) + ddx(Q_{jCi}, V(bi)) \\ ((-1)ddx(Q_{dEi}, V(ei)) + (-1)ddx(Q_{dCi}, V(ci))) \quad , \tag{7.4.0-38}$$

and

$$Q_{rBi} = C_{rBi} V(bp, bi) . \tag{7.4.0-39}$$

7.5 Correlated noise implementation

As per discussion in section 2.1.14.1 the implementation of correlated noise is not straight forward in ***Verilog-A***. In Verilog-A only a limited number of functions are supported for noise simulation, among which *"white_noise()"* and *"flicker_noise()"* are useful and permit correlated noise implementation for a real valued correlation coefficient only. However, one can use the *"ddt()"* operator with a concept of capacitive coupling to implement any imaginary correlation. The main problem according to (2.1.13.1-1) is to implement the noise source in the output with the proper PSD, part of which depends upon the square of the frequency proceeded by a negative sign. Hence, an approximate expression has been used as in (2.1.13.1-4) to resemble the theoretical solution as much as possible. For ease of explanation writing down the same approximated expression here once more,

$$S_{\underline{i_{nc}}} = S_{i_{nc}} \left(1 - B_f \left(\omega \frac{\tau_{Bf}}{3}\right)^2\right)^2 = S_{i_{nc}} - |t_{21}|^2 S_{i_{nb}} + \underbrace{\frac{|t_{21}|^4}{4B_f} S_{i_{nb}}}_{\text{error term}} , \tag{7.5.0-40}$$

with B_f as d.c. gain.

In equation (7.5.0-40), the factor 1/3 results from the same series expansion as for the transfer current related NQS effect in the base of a pure diffusion transistor. Therefore, the corresponding parameter "alit" is used instead of the factor 1/3.

Three shot noise sources have to be implemented: the regular one and one with the correlation impact for the transfer current, and a regular one for the base current. In addition, two dummy noise current sources are created with spectral densities $2 \cdot q \cdot i_{bei}$ and $2 \cdot q \cdot i_T$ at (n1, 0) and (n2, 0) branches. Connecting with 1Ω resistor, it has been ensured that noise currents are the same as the noise voltages at the respective branches.

The transfer current related noise sources have to be implemented as controlled sources by tagging a capacitor (representing the noise correlation time) to the input noise source in order to obtain the frequency dependence. The corresponding equivalent circuit is shown in Fig. 7.5.0/8. The upper part contains the three noise sources while the two networks in the lower part of the figure are used for realizing the correlation expression. The equations for the three noise sources read,

$$I(bi, ei) = gV(b\_\mathrm{n1}), \tag{7.5.0-41}$$

$$V(b\_\mathrm{n1}) = \frac{1}{g}\sqrt{2 \cdot q \cdot i_{bei}}, \tag{7.5.0-42}$$

$$I(ci, ei)_1 = \left(1 - \frac{B_f}{2}(alit \cdot Tf \cdot \omega)^2\right) \cdot g \cdot V(b\_n2), \tag{7.5.0-43}$$

$$V(b\_n2) = \frac{1}{g}\sqrt{2 \cdot q \cdot i_T}, \tag{7.5.0-44}$$

$$I(ci, ei)_2 = -j\omega \cdot B_f \cdot alit \cdot Tf \cdot g \cdot V(b\_n1). \tag{7.5.0-45}$$

Here, g corresponds to a uniform conductance of 1S. $\mathrm{I(ci,ei)}_2$ indeed represents the negative contribution caused by the correlation while $\mathrm{I(ci,ei)}_1$ includes the (undesired) error term resulting from the approximation (7.5.0-40).

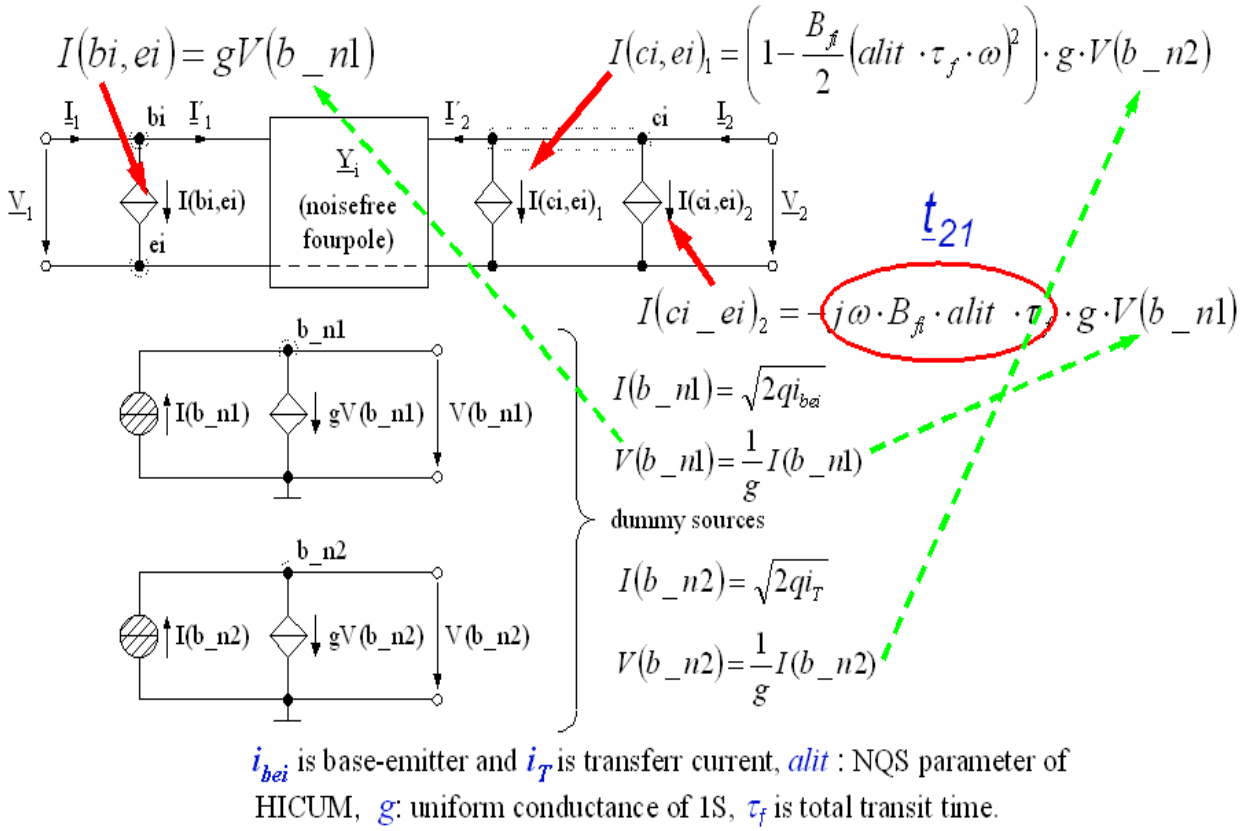

Fig. 7.5.0/8: Equivalent circuit used for implementing noise correlation. The lower two networks (labelled as dummy sources) are used for realizing the PSD for base and collector currents.

The implementation was experimentally verified on SiGe HBTs. To provide a feeling for the relevance of correlated noise and the accuracy of the implemented noise correlation model, examples are shown in Fig. 7.5.0/9 and Fig. 7.5.0/10 for a SiGe HBT with peak transit frequency of 150GHz (emitter area 0.2*10.16μm^2, CBEBC configuration). The correlation has its biggest impact on the minimum noise figure NF_{min} and the real part of the optimum source reflection coefficient Γ_{opt}. The importance of the correlation increases with frequency. The results show that HICUM with the implemented noise correlation agrees quite well with measured data.

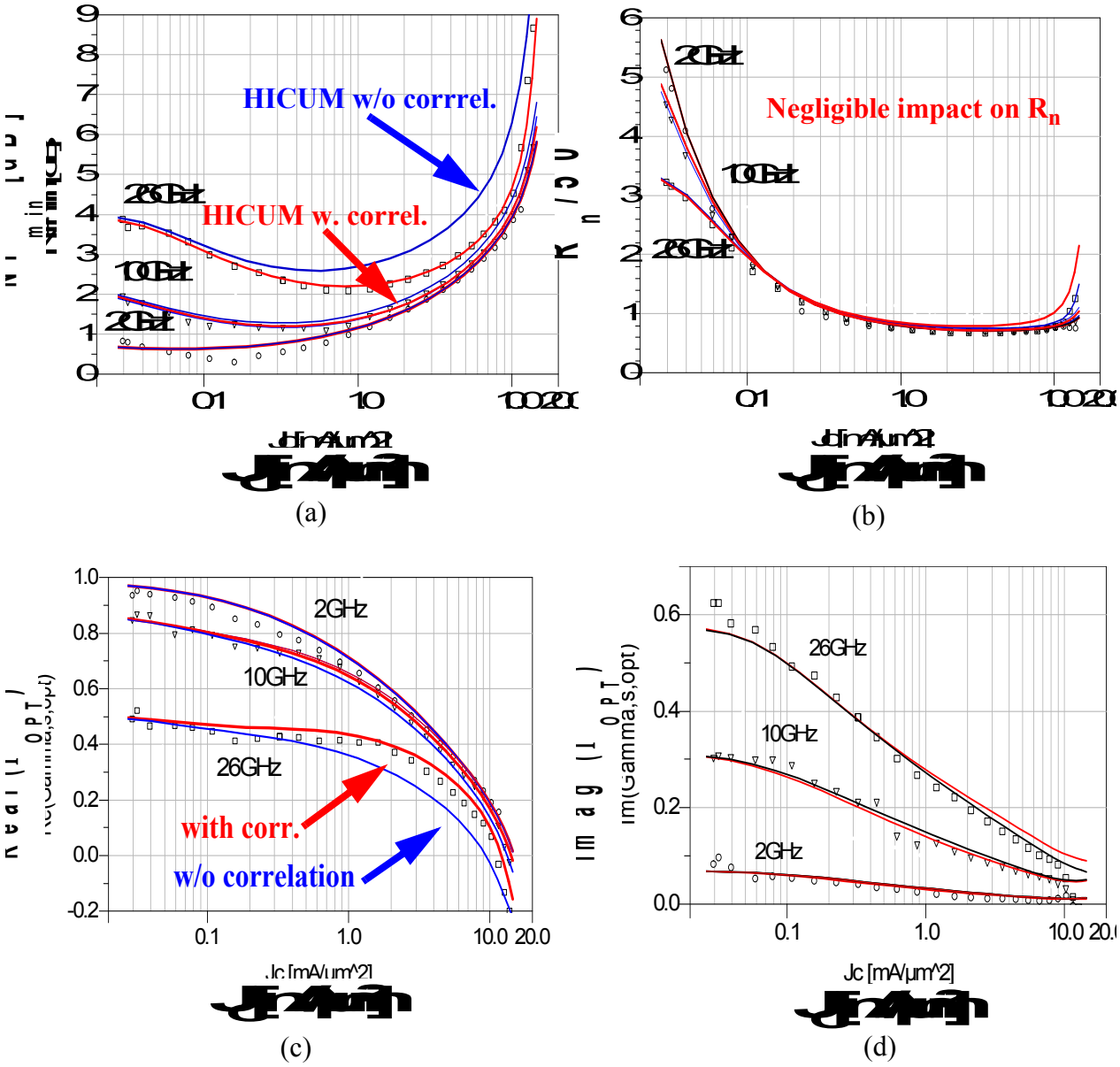

Fig. 7.5.0/9: Comparison of measured noise parameters (symbols) with simulated data from HICUM without correlation (blue lines) and with correlation (red lines). (a) Minimum Noise factor; (b) Equivalent noise resistance; (c) real and (d) imaginary part of optimum source reflection coefficient. The hardware was provided by Jazz Semiconductor.

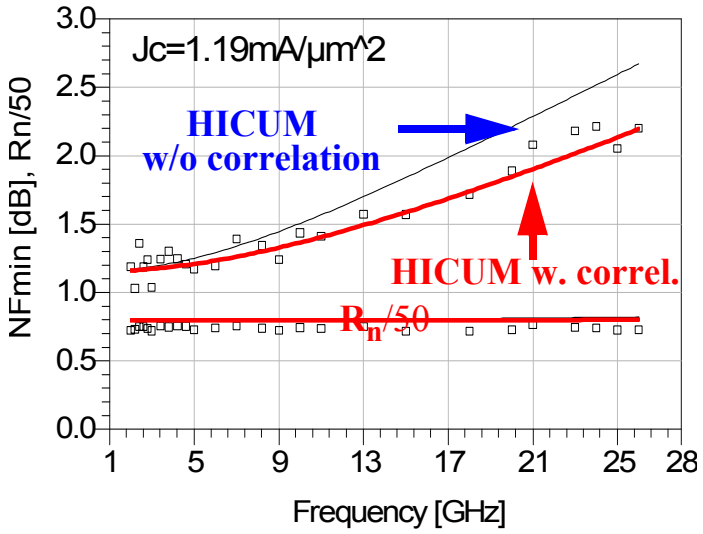

Fig. 7.5.0/10:Frequency dependence of NF_{min} and R_n at the optimum bias point in terms of noise.